GeoScienceWorld
Lithosphere
Volume 2022, Article ID 6725334, 16 pages
https://doi.org/10.2113/2022/6725334

Lithosphere

Research Article

Experimental Study on the Failure Characteristics and Damage Evolution of Sandstones from Typical Buried Depths in High In Situ Stress Area

Yi-hang Li,[1] **He-ping Xie**,[1,2] **Gan Feng**,[1,3] **Ru Zhang**,[1] **Guang-ze Zhang**,[4] **Zheng-xuan Xu**,[4] **Tao Feng**,[4] **Dong Wang**,[4] **Xiao-juan Yi**,[4] **Ming-hao Chen**,[4] **An-lin Zhang**,[1] **Zhi-long Zhang**,[1] **and Li Ren**[3]

[1]*State Key Laboratory of Hydraulics and Mountain River Engineering, College of Water Resource and Hydropower, Sichuan University, Chengdu 610065, China*
[2]*Shenzhen Key Laboratory of Deep Engineering Sciences and Green Energy, College of Civil and Transportation Engineering, Shenzhen University, Shenzhen 518060, China*
[3]*Key Laboratory of Deep Earth Science and Engineering (Sichuan University), Ministry of Education, Sichuan University, Chengdu 610065, China*
[4]*China Railway Eryuan Engineering Group Co. Ltd., Chengdu 610031, China*

Correspondence should be addressed to Gan Feng; fenggan@whu.edu.cn and Li Ren; renli@scu.edu.cn

Received 19 April 2022; Accepted 16 July 2022; Published 9 August 2022

Academic Editor: Xiaoding Xu

This study is aimed at exploring the mechanical properties and failure characteristics of the rocks surrounding a railway tunnel in Qinghai-Tibet Plateau at typical buried depths. Uniaxial compression and AE experiments were carried out on sandstones taken from the same borehole. The results show that the elastic modulus and peak strength of the 750 m depth sandstones are much higher than those of the 350 m depth sandstones. The crack evolution in the 750 m depth sandstones was more orderly, and its brittle failure characteristics were more obvious as compared with the 350 m depth sandstones. The fractal dimension of the samples from the typical depths reached the minimum value when the fracture volume state changed from compression to expansion. In addition, the damage variable based on the crack volumetric strain theory (D_C) and cumulative ring counts of acoustic emission (D_A) can, respectively, reflect the generation and penetration of cracks and the physical properties of rocks at the two typical depths. The combination of D_C and D_A can be used to analyze the evolution of the sandstone's damage. The research results have basic theoretical significance for the excavation and geological disaster prevention of tunnels in sandstone sections at typical depths in the Qinghai-Tibet Plateau.

1. Introduction

The increasing development of traffic engineering has led to the emergence of increasingly longer and deeper tunnels. In southwestern China, the complex geological environment poses significant tunnel engineering challenges due to the great terrain elevation differences, strong plate activity, and frequent mountain disasters [1]. In the Hengduan Mountain area along the Sichuan-Tibet Tunnel, the geological tectonic movement is intense, and the environment here is characterized by high in situ stress. Studies [2–15] have shown that the mechanical properties of rocks are affected by environmental factors such as temperature, ground stress, humidity, and water content. These environmental factors are all related to the buried depth of the rocks and especially so in Qinghai-Tibet Plateau, where the tunnel length is long and the tunnels often pass through formations with large depth differences. The mechanical properties and failure characteristics of rocks are critical factors in the analysis of the stability of surrounding rocks. Therefore, the study of rock

deformation and instability processes at different depths is of great significance in the damage evaluation of the surrounding rocks and in disaster prevention in tunnel engineering.

The mechanical properties of rocks at different depths are different. At present, for soft rock (take coal as an example), in terms of physical parameters, Xie et al. [16] concluded that coal rock at large depths has higher compressive strength and greater plasticity than those at shallower depths, making it more difficult to control the stability of the roadway's surrounding rock. Zhang et al. [17] concluded that with the increase in the effective stress, the porosity and permeability of coal samples at different depths decreased in a negative exponential function. Jia et al. [18] carried out an unloading failure test of coal obtained from a depth of 300-1050 m and concluded that the acoustic emission (AE) energy release trend, energy dissipation, and dissipation efficiency all correlate well with the increase in depth and that the failure of deep coal is more intense. For hard rock, Lu et al. [19] conducted uniaxial compression experiments on rocks obtained from a large buried depth of 1000~6400 m and found that their compressive strength showed a nonlinear logarithmic increase with depth and that the elastic modulus, Poisson's ratio, and compressive strength were all negatively correlated with the content of the weak phase minerals. Nonetheless, the existing researches on the mechanical properties of rock at different depths mainly focus on the mining of deep resources. After all, one tunnel in the southwest plateau area of China will span multiple buried depths, and there is a lack of research on the surrounding rock at typical buried depths of tunnel engineering in high-altitude and high in situ stress areas.

Besides, most of the research focuses on the research on physical parameters and apparent characteristics and lacks the analysis of the full failure process of the rock and the characterization of feature points. Rock failure is a direct manifestation of its mechanical response. Martin [20] analyzed the failure of brittle rocks and showed that the brittle-failure process is characterized by a loss of cohesion as the friction is mobilized. Gao et al. [21] showed that the propagation of initial cracks has a great influence on the failure process of a rock slope and proposed a new fracture criterion for cracked rock. Feng et al. [22, 23] studied the fracture characteristics of dense granite under a thermal cycle and obtained that rapid cooling promotes the generation of rock cracks and has a significant impact on fracture resistance. Tang et al. [24] showed that the internal cause of rock failure was the sudden release of the elastic energy stored in the rock mass. After anchoring, the mechanical properties of the specimen were significantly improved after the peak strength was reached, and more strain energy was absorbed. Hajiabdolmajid et al. [25] observed that brittle failure is mainly a progressive spalling process, which leads to the failure of the rock mass' structure in the form of a V-notch in many cases. Many scholars have simulated various environmental and engineering conditions in the laboratory and carried out a lot of research on rock mechanical response [26–38]. However, there is a lack of analysis of the failure process of the surrounding rock at different buried depths in tunnel engineering. Due to the influence of strong geological tectonics, the instability and failure process of the surrounding rock in the Qinghai-Tibet Plateau is very complex, which is manifested by the occurrence of frequent geological disasters that are difficult to effectively and accurately predict.

As a nondestructive monitoring method, acoustic emission is commonly used in rock failure prediction under disturbance. Therefore, in the study of rock mechanics, acoustic emission monitoring methods are often used to study the rock failure properties, failure laws, mechanical behavior, and so on, as well as the relationship between rock mechanical properties and acoustic emission characteristics [39–44]. Lockner et al. [45] stabilized the failure process of brittle rock by controlling the stress to maintain a constant acoustic emission rate and provided a detailed view of fault nucleation and growth processes through the analysis of the arrival time and amplitude of acoustic emission signals; they also combined the cumulative event count of acoustic emission signals with the damage mechanics model to determine how damage accumulates during loading to predict rock instability [46]. Liu studied the synergistic characteristics of acoustic emission in the process of rock failure by investigating the relationship between the internal change of a rock mass' structure and its acoustic emission characteristics and verified the accuracy of the acoustic emission evolution equation and the feasibility of using rock acoustic emission. He et al. [47] found that when the limestone sample was under low stress, the acoustic emission signal had the characteristics of high frequency and low amplitude, and when the sample was near the condition of rock fracture and failure, the acoustic emission signal had high amplitude and low frequency.

It can be seen that scholars have achieved rich results regarding the influence of different buried depths on the physical and mechanical properties of rocks and the deformation and failure processes of surrounding rocks. For the tunnels in Qinghai-Tibet Plateau, where the surrounding rock of tunnels is affected by the strong geological structure and special geological conditions, the prediction and control of the stability of the surrounding rock in tunnels are fraught with challenges such as an unclear understanding of the mechanical properties and failure characteristics of the surrounding rock, making it difficult to predict when the surrounding rock will fail. At present, there is a lack of studies on the failure process and damage evolution of the surrounding rock at different depths in the large and deep tunnels in the Qinghai-Tibet Plateau. Therefore, in this study, an MTS815 Flex test GT electrohydraulic servo rock mechanics test system and a PCI-2 acoustic emission system were used to carry out uniaxial compression failure tests on sandstone samples from a railway tunnel in Qinghai-Tibet Plateau. Based on the crack volumetric strain, failure properties, and strength deformation of the sandstone samples, the differences in their mechanical parameters, mechanical properties, and mineral composition at different depths and the factors influencing these characteristics were studied to understand their damage evolution process.

FIGURE 1: Geological location map of sampling site.

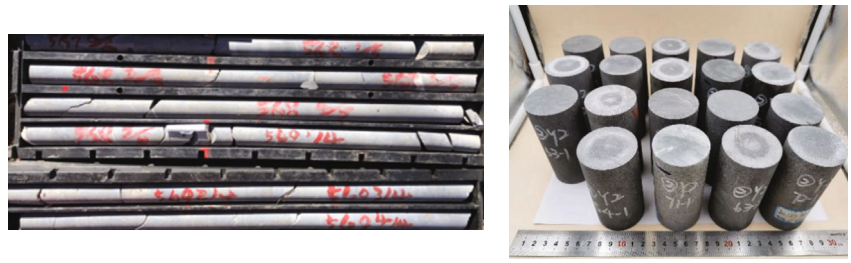

(a) (b)

FIGURE 2: Sandstone cores and sample specimens. (a) Core obtained from field drilling. (b) Standard specimens made from rock cores.

2. Experimentation

2.1. Sample Preparation. The sampling site is located in a tunnel in Yajiang County, eastern Qinghai-Tibet Plateau (Figure 1), with an altitude of 3500 m. The drilling depth is 890 m. The lithology of the tunnel's surrounding rock is mainly sandstone and slate, as shown in Figure 2(a).

The samples were collected from high-altitude areas with high in situ stress. Most of the cores sampled by field drilling were relatively broken, and the coring rate was low. After geological exploration and testing, the lithology of the 350 m and 750 m buried depths is sandstone. In order to ensure that a certain number of standard samples can be produced and at the same time to maintain the consistency of lithology, considering the site selection and buried depth of the tunnel, sandstone samples from 350 m and 750 m were selected as typical buried depth rock samples for analysis.

The sandstone cores from 350 m and 750 m depth were selected to prepare several standard cylindrical specimens with a diameter of 50 mm and a height-diameter ratio of 2 : 1, as shown in Figure 2(b). During the machining process, the diameter deviation of the upper and lower ends of the

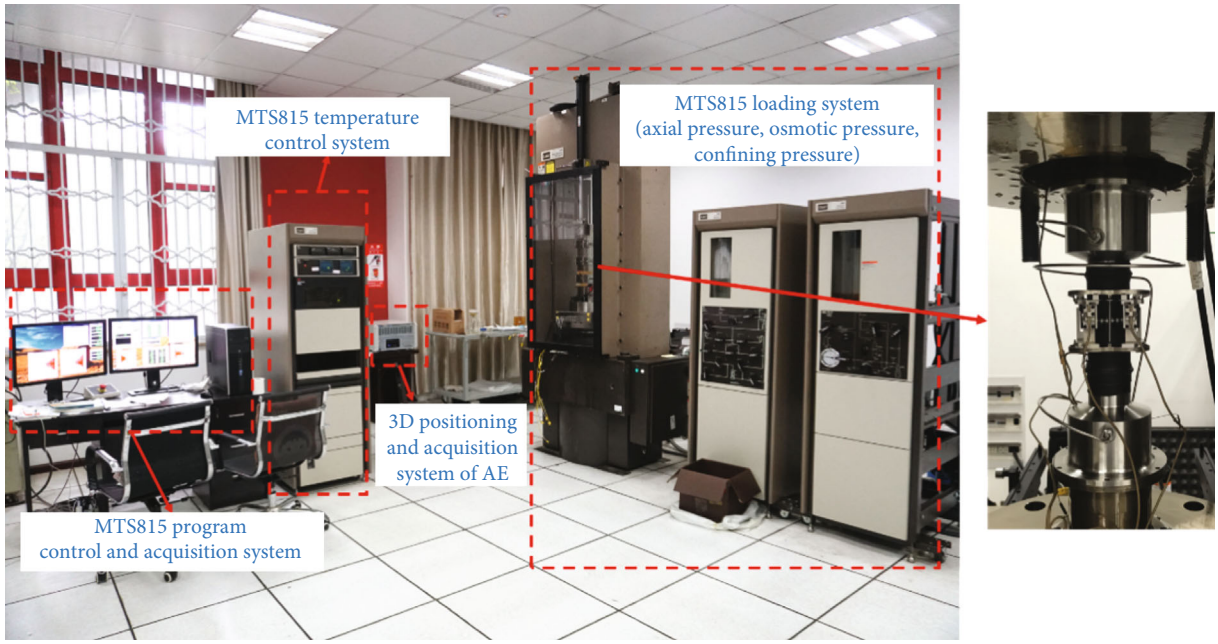

Figure 3: MTS 815 Flex test GT test system.

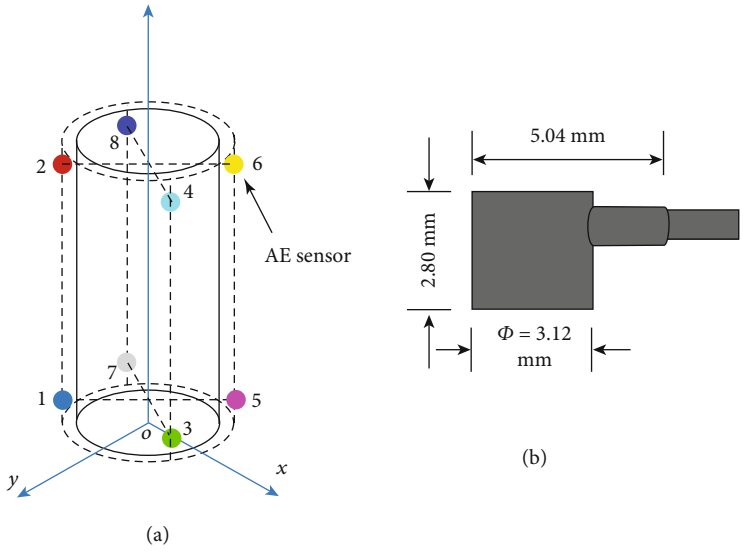

Figure 4: Layout and schematic diagram of acoustic emission sensors. (a) Spatial arrangement of the acoustic emission sensors on the sample. (b) Acoustic emission sensor.

specimen was controlled to be less than 0.2 mm, the axial deviation was less than 25°, and the parallelism was less than 0.05 mm. The average density of the sandstones at 350 m and 750 m depth is 2683.99 kg/m^3 and 2719.56 kg/m^3, respectively.

2.2. Mechanical Experiments. The uniaxial compression experiment was carried out using the MTS 815 Flex test GT test system of Sichuan University (Figure 3). The displacement loading mode was set at a loading rate of 0.1 mm/min.

The acoustic emission test was conducted using the PCI-2 acoustic emission monitoring system of PAC Company, USA. The system can simultaneously capture the AE timing features and locate the AE space. Eight AE sensors were evenly distributed at the upper and lower ends of the specimen. In order to eliminate the signal interference generated during the initial loading, the AE sensors were polished at the contact part of the specimen. Vaseline was applied at the contact position to ensure good coupling between the AE sensors and the sample. The arrangement of the acoustic emission sensors on the rock samples is shown in Figure 4.

3. Experimental Results and Analysis

3.1. Stress-Strain Curve. During the uniaxial compression experiments of the sandstones, the load and displacement data were automatically recorded by a computer, and the

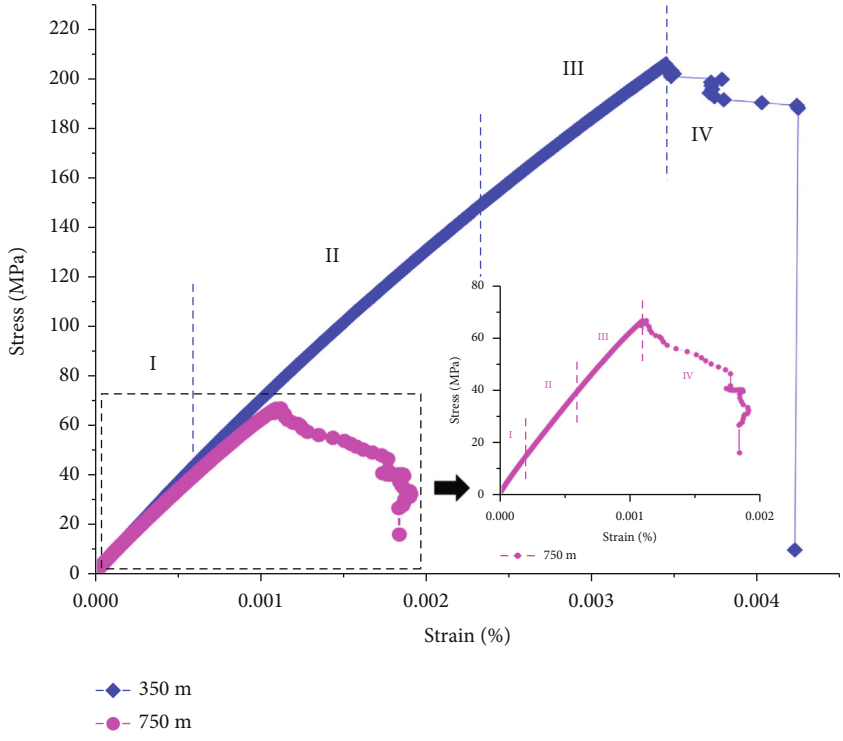

Figure 5: Typical stress-strain curves of samples at 350 m and 750 m depths.

stress-strain curve was obtained. The typical stress-strain curves of the samples from the 350 m and 750 m depths were selected and plotted as shown in Figure 5.

The compression failure process of the rock specimens is generally divided into 4 stages: I compaction stage, II elastic compression stage, III plastic stage, and IV failure stage. After the initial compaction stage, the sandstone samples in this experiment basically maintained the elastic compression state, during which there was no obvious yield and inelastic deformation, until the peak stress. The slope of the stress-strain curve decreased in the plastic stage; because most of the rocks in high-altitude areas were hard and brittle rocks, the plastic stage was not obvious. The specimens from the 750 m depth rapidly failed after the peak stress, showing obvious brittle failure characteristics. The specimens from the 350 m depth showed a ladder drop trend after the peak stress. This may be because, in the rock samples from the shallower buried depth, the primary cracks were relatively developed, and in the compression process, the microcracks expanded but did not penetrate. Therefore, they still had a certain bearing capacity after the peak stress, after which new cracks propagated, resulting in a small decrease in the stress; this phased stress reduction led to the ladder drop trend of failure [48].

The mechanical parameters of the sandstone at the different depths were calculated, and the average value was taken, as shown in Table 1. The peak stress (σ_p) and the elastic modulus (E) of the sandstones from the 750 m depth are higher by 204.3% and 15.4%, respectively, as compared with that of the sandstones from the 350 m depth. This may be because the sandstones from the 750 m depth are more affected by the in situ stress and the tectonic stress than the sandstones from the 350 m depth, resulting in sandstones that are denser and have more brittle properties and higher strength.

Table 1: Mechanical parameters obtained from the uniaxial compression tests.

Depth (m)	E (GPa)	μ	σ_p (MPa)
350	61.60	0.167	74.82
750	71.08	0.217	227.73

3.2. AE Feature Analysis. In the process of acoustic emission monitoring, the AE characteristic data were recorded, and the AE energy time series evolution curve of the sandstone samples was drawn. The typical curves were selected for different depths, as shown in Figure 6.

It can be seen from Figure 6 that there is no obvious AE energy generation in the initial compaction stage of the sandstone sample from the 350 m depth, and sporadic high AE energy generation occurs in the elastic compression stage. Before the peak load of the sample from the 750 m depth, a small number of low AE energy events occur. A certain amount of secondary cracks were produced after the rock samples from the high buried depth were removed from their environment, resulting in a reduction in the energy released by the main fracture; this is related to the original environment of the rock, its microstructure, and the fracture evolution of the rock. All the sandstone samples suddenly generated a large number of AE events with large energy when they reached the peak stress. This is due to

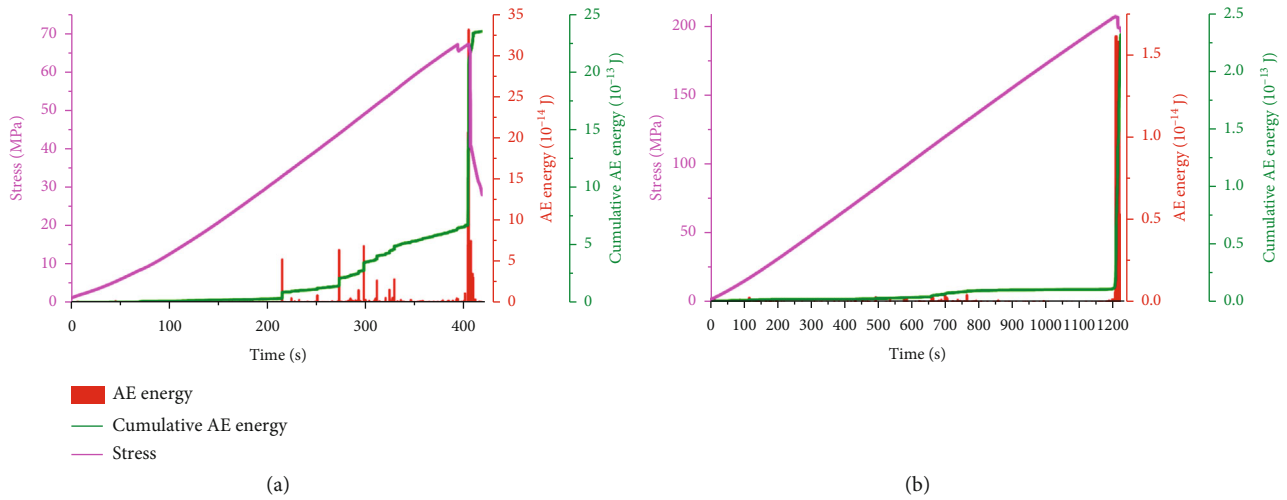

Figure 6: AE energy temporal evolution curve: (a) 350 m; (b) 750 m.

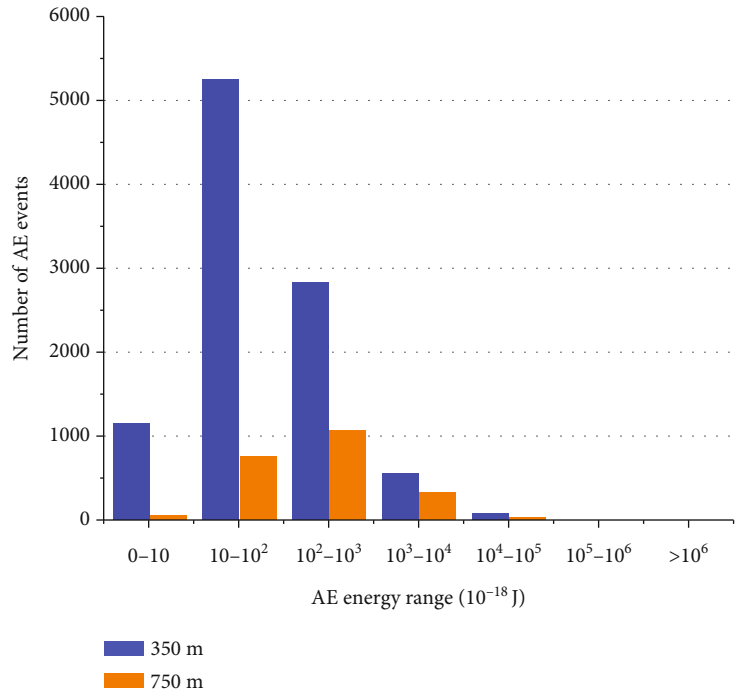

Figure 7: Distribution of the number of AE events in each energy interval.

the aggregation and penetration of a mass of microcracks, the formation of macroscopic cracks, and the loss of the main bearing capacity of the rock. The stored elastic energy was released, and a large amount of energy was captured by the acoustic emission probes.

Figure 7 shows the distribution of AE energy and the number of AE events. It can be clearly seen that the number of events of each energy level and the average energy of the deep rocks are far less than those of the shallow rocks. According to the Cottrell dislocation pile-up model theory [49], the original defects of sandstone will slip under uniaxial compression. However, due to the small particle size and high hardness of the sandstones from the 750 m depth, the bonding force between the rock particles is strong, the movement between particles is blocked, and the dislocations in the crystal accumulate on the grain boundaries. With the continuous accumulation of defects, the crystal dislocation movement of the deep sandstone is greatly resisted, and a certain amount of elastic energy accumulates inside the rock. When this energy is released, the phenomenon of high energy level, small number of AE events, and low total energy of acoustic emission events appears. In the acoustic emission monitoring data, the number of acoustic emission events of sandstones from the 350 m depth in each energy level is significantly greater than that of the sandstones from the 750 m depth, but the proportion of acoustic emission

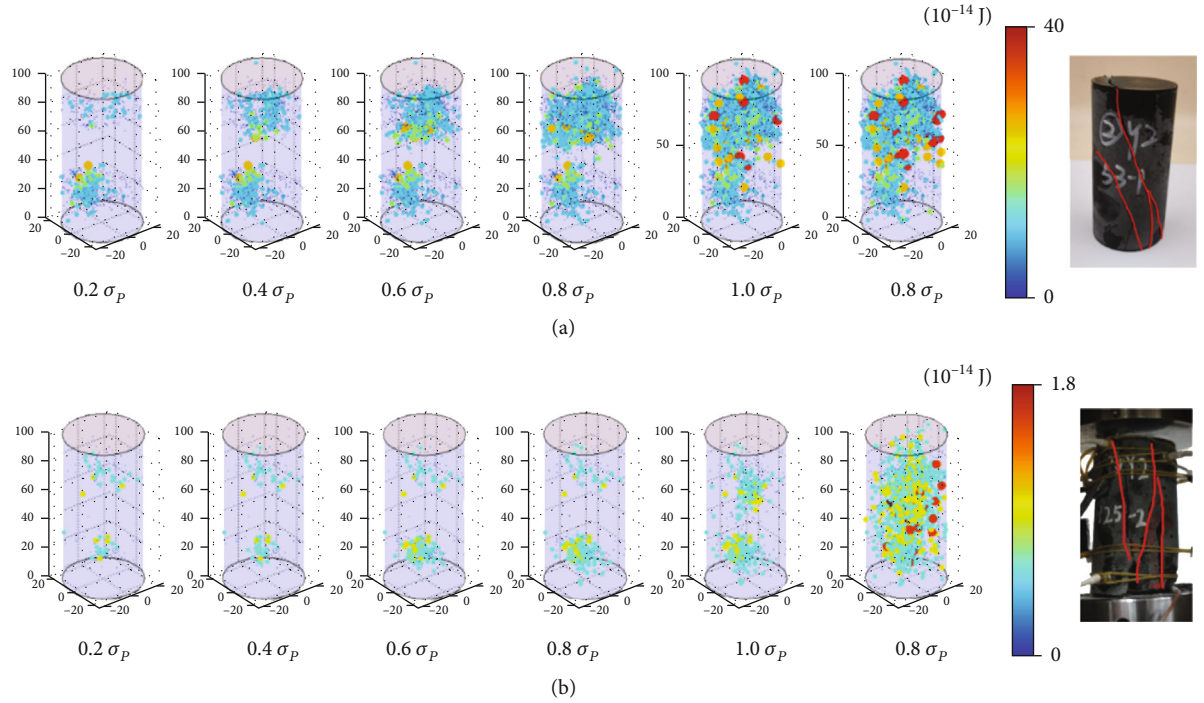

Figure 8: AE spatial distribution evolution and failure mode of sandstone samples: (a) 350 m; (b) 750 m.

events in the 10~103 aJ energy level (1 aJ = 10^{-18} J) is significantly lower than that of the latter.

Multiple acoustic emission probes can be used to locate the position of acoustic emission events so as to clearly show the fracture state of the rock in each stress stage and the development trend of the fractures. The typical spatially located fracture processes of the sandstones at different depths are shown in Figure 8.

Figure 8 shows the AE spatial distribution evolution and failure mode of the 350 m and 750 m depth sandstone samples. The sphere inside the sample represents the acoustic emission event, and its size and color represent the corresponding energy. All sandstone samples produced some acoustic emission events at the end of the initial compaction stage, indicating that the rock produced microcracks at the end under uniaxial compression. Then, with the increase in the axial stress, the microcracks began to nucleate and form through cracks, and the samples lost their bearing capacity after reaching peak stress, resulting in a large number of high-energy acoustic emission events. The failure mode of the sandstone samples from the 350 m depth is mainly shear failure, and there are some tensile cracks at the end of the samples. The failure mode of the sandstone samples from the 750 m depth is tensile failure parallel to the axial direction, accompanied by the shedding of some shear surfaces. The failure modes of the sandstone samples from different depths are obviously different under uniaxial compression. Compared with the corresponding acoustic emission event location map of rock samples from different depths, it is obviously seen that the acoustic emission event data points at the corresponding position are more concentrated, forming a similar fracture surface.

Under the condition of uniaxial compression, the macrocracks after rock failure were mostly vertical cracks caused by the tensile stress in the horizontal direction. Figure 8 divides the whole process of the experiments according to the percentage of peak strength. By comparing the number and distribution characteristics of acoustic emission events in different stress segments, the evolution process of the samples during the failure process could be obtained. As can be seen from Figure 8, the acoustic emission events were initially concentrated at the end of the samples. With the increase of stress, the acoustic emission events began to concentrate on the failure surface, and the cracks gradually developed and penetrated the dense areas of the acoustic emission events, resulting in the fracture surface. The sandstone samples produced sudden and concentrated acoustic emission events when the stress reaches 80%-100% compressive strength. The high-energy acoustic emission events in the rock samples from 350 m depth mainly occurred in the middle and upper parts, forming an obvious AE event concentration zone, which led to the formation of local shear weak planes. Finally, the shear cracks penetrated, resulting in macroscopic shear failure. When in 750 m, a lot of high-energy acoustic emission events occurred in the postpeak stage, which was scattered in the middle and side walls of the rock samples, causing the rock samples to splitting failure with slight shear plane fracture. It can be inferred that the large number of acoustic emission events at the ends of the rock samples at both depths in the initial stage was the generation of tension microcracks. The 350 m's rock samples began to generate high-energy shear microcracks after the stress reached 80% of the uniaxial compressive strength and quickly penetrated to form a fracture surface. The

750 m's rock samples produced plenty of tensile fractures with a small proportion of shear fractures in the postpeak stage.

3.3. Crack Volumetric Strain and Fractal Dimension Analysis

3.3.1. Calculation of Crack Volumetric Strain. The deformation of rock materials is often accompanied by the stages of crack closure, initiation, propagation, and penetration [50, 51]. Martin and Chandler [52] proposed a crack volumetric strain calculation method through a study of granite, and it has been widely used by scholars around the world [53, 54]:

$$\varepsilon_1^c = \varepsilon_1 - \varepsilon_1^e = \varepsilon_1 - \frac{[\sigma_1 - \mu(\sigma_2 + \sigma_3)]}{E}, \quad (1)$$

$$\varepsilon_2^c = \varepsilon_2 - \varepsilon_2^e = \varepsilon_2 - \frac{[\sigma_2 - \mu(\sigma_1 + \sigma_3)]}{E}, \quad (2)$$

$$\varepsilon_3^c = \varepsilon_3 - \varepsilon_3^e = \varepsilon_3 - \frac{[\sigma_3 - \mu(\sigma_1 + \sigma_2)]}{E}. \quad (3)$$

According to Equations (1)–(3), the crack volumetric strain $\varepsilon_v{}^c$ of a rock mass is obtained:

$$\varepsilon_v = \varepsilon_1 + \varepsilon_2 + \varepsilon_3, \quad (4)$$

$$\varepsilon_v^c = \varepsilon_1^c + \varepsilon_2^c + \varepsilon_3^c = \varepsilon_v - \frac{1 - 2\mu}{E}(\sigma_1 + \sigma_2 + \sigma_3), \quad (5)$$

where ε_V is the volumetric strain of the rock. In the experiments of this paper, $\sigma_2 = \sigma_3$.

According to Equation (5), combined with the relevant data measured by the tests, the crack volumetric strain in the process of rock failure can be obtained.

3.3.2. Fractal Dimension Calculation of Spatial Distribution of AE Events. Experiments show that the acoustic emission sequence of rock materials has fractal characteristics in space and that the fractal dimension is an important characteristic parameter to reflect the fractal structure, which can quantitatively describe the complexity of the internal structure of things [55]. The box dimension can be defined as:

$$N(r) = Cr^{-D}, \quad (6)$$

where $N(r)$ is the number of discrete bodies whose characteristic size is greater than r, r is the radius covering natural discrete bodies, and C is the material constant. Another form of Equation (6) is the number-radius relationship:

$$M(r) = Cr^{-D}, \quad (7)$$

where $M(r)$ is the number of bodies contained in a circle with radius r. If the discrete body has a fractal distribution, it satisfies Equation (7). Taking logarithms on both sides of Equation (7) at the same time, the following can be obtained:

$$\lg M(r) = \lg C + D \lg r. \quad (8)$$

The $\lg M(r)$-$\lg r$ curve is drawn in logarithmic coordinates, and its linear segment is fitted by the least square method. If the fitting results of the two variables have a good linear correlation, it can be considered that the distribution of the AE spatial location points under different loads has self-similarity in the damage evolution process of specimens. The dimension D derived from Equation (8) is called cluster dimension.

3.3.3. Variation of Crack Volumetric Strain and Fractal Dimension. Figure 9 shows the variation curves of the crack volumetric strain and the fractal dimension of the sandstone samples from the different depths. According to the crack volumetric strain curve, the point where the crack volumetric strain changed from compression to expansion is named the "Turning Point."

It can be seen from Figure 9 that the fractal dimension of the sandstone samples from the different depths decreases first and then increases with the loading process, while the crack volumetric strain decreases first and then expands. The Turning Point of the crack volumetric strain from compression to expansion has a good matching relationship with the lowest point of the fractal dimension, and the Turning Point appears slightly earlier than the lowest point of the fractal dimension. A large spatial fractal dimension indicates a disordered and random distribution of cracks. A small spatial fractal dimension indicates that the cracks are becoming stable and orderly, thus further resulting in the formation of a large rupture.

When the spatial fractal dimension is the smallest, it means that the generation of cracks has the most regularity. At this time, the crack volume state generally changes from compression to expansion, indicating that the speed of crack penetration and expansion in the rock has exceeded the speed of crack closure, which further indicates that the main fracture surface or the main crack has begun to form. Subsequently, the crack propagation in the rock will be accelerated to generate penetrating cracks along the previously formed main fracture surface [56]. With the expansion of the crack volume, the internal structure of the rock is irreversibly damaged, and the overall brittle instability occurs under peak load. This process returns the interior to a chaotic, random state, so the fractal dimension begins to increase.

Comparing the fractal dimensions of the samples from different depths presented in Figure 10 shows that the fractal dimension of the sandstones from the 750 m depth maintained a significantly lower level (below 1.5) during the entire loading process than the sandstones from the 350 m depth. This shows that the overall evolution of internal cracks in the deep rock samples is more orderly and stable, and its distribution is more concentrated. Therefore, the uniaxial compression failure of the deep rock samples is more sudden and brittle.

There are few primary fractures in the sandstones from the 750 m depth, but the volumetric strain value corresponding to the Turning Point is significantly greater than that of the sandstones from the 350 m depth, which indicates that massive secondary cracks were produced in the sandstones from the 750 m depth after leaving the original environment

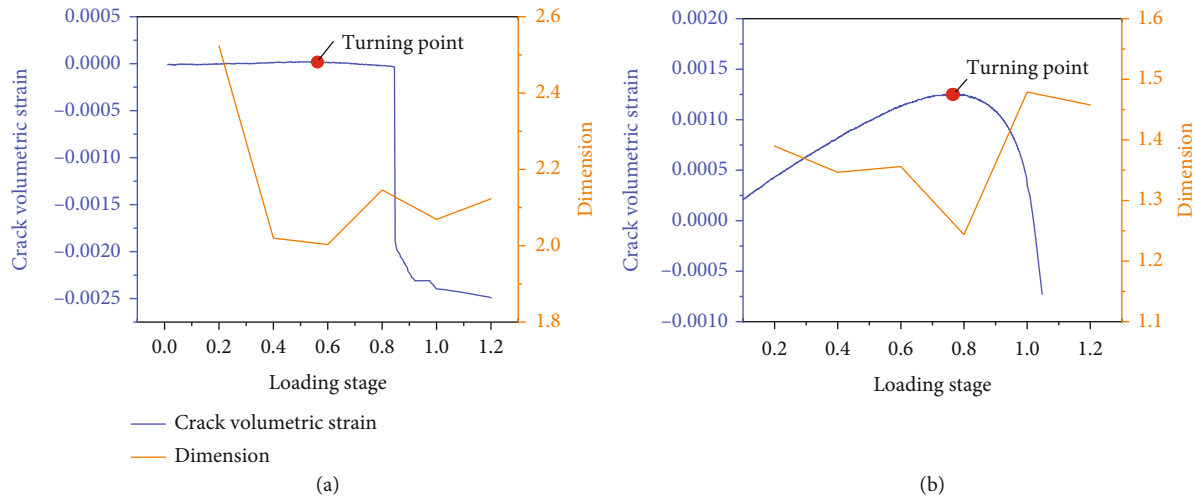

FIGURE 9: Variation curves of crack volumetric strain and fractal dimension of sandstone samples: (a) 350 m; (b) 750 m.

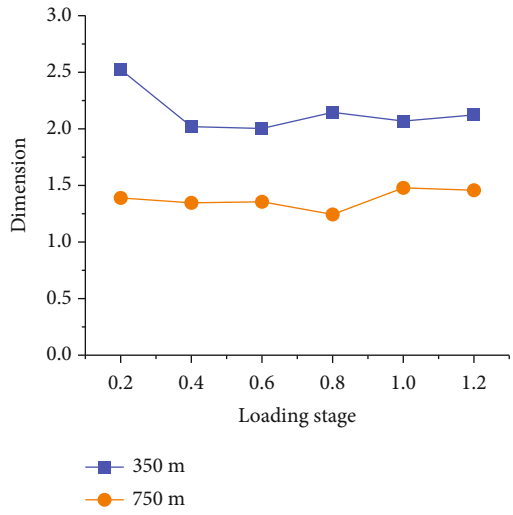

FIGURE 10: Comparison of the fractal dimension of sandstones at different depths.

[57, 58]. This may be because when the core was drilled, the sandstone broke away from the in situ stress environment, and the stress was suddenly released, resulting in the generation of a large volume of secondary cracks. The secondary cracks are often parallel to the expansion direction of the original cracks, and the additional free surface formed is much smaller than that of the original cracks, so the energy needed to crush these cracks is lower. The secondary cracks of different cleavage planes form cleavage steps because of the height difference of each plane. After being compacted, the energy released by the main fracture will be reduced. This also explains the certain number of discontinuous and low-energy AE events in the compaction stage and elastic stage of the sandstone samples from the 750 m depth in Figure 5. In addition, this phenomenon further shows that it is of great significance to retain the original in situ environment when coring [59].

4. Damage Evolution Analysis of Sandstones

The crack propagation and evolution of rock have a significant impact on the mechanical properties and failure characteristics of rock. It is necessary to study the damage to rock under different conditions [60–62]. Sandstones at different depths have different degrees of brittleness before peak stress. Microscopically, microcracks are formed, propagated, and converged; that is, the cleavage force is less than the slip force but greater than the debonding force. After the destruction of the valence bond between atoms, a cleavage plane is formed and microcracks are gradually generated. The brittle rock usually does not undergo obvious plastic deformation macroscopically, but its damage localization degree is high. Therefore, it is necessary to define the damage variable to describe this damage.

AE is the release of elastic waves generated during the damage process; it can reflect the damage degree of rock to a certain extent and is also related to the internal defects of the rock and its inversion process. According to Kachanov's theory [63], on the further derivation of the defect area, the AE cumulative ring count can be used as a characteristic parameter to characterize the damage variable, namely,

$$D_A = \frac{N_d}{N_m} = 1 - \exp\left(-\frac{\varepsilon^m}{\alpha^m}\right), \tag{9}$$

where D_A is the damage variable characterized by the AE cumulative ring count, N_d is the cumulative acoustic emission ring count in the process of rock failure, N_m is the cumulative acoustic emission ring count when the entire section is completely destroyed, and α, m are the binary parameters of the Weibull distribution of infinitesimal strength.

Zong et al. [64, 65] proposed that expansion in rock is the result of the generation and propagation of microcracks in the rock, reflecting the damage to the rock under external load. Therefore, in this study, the Turning Point is proposed

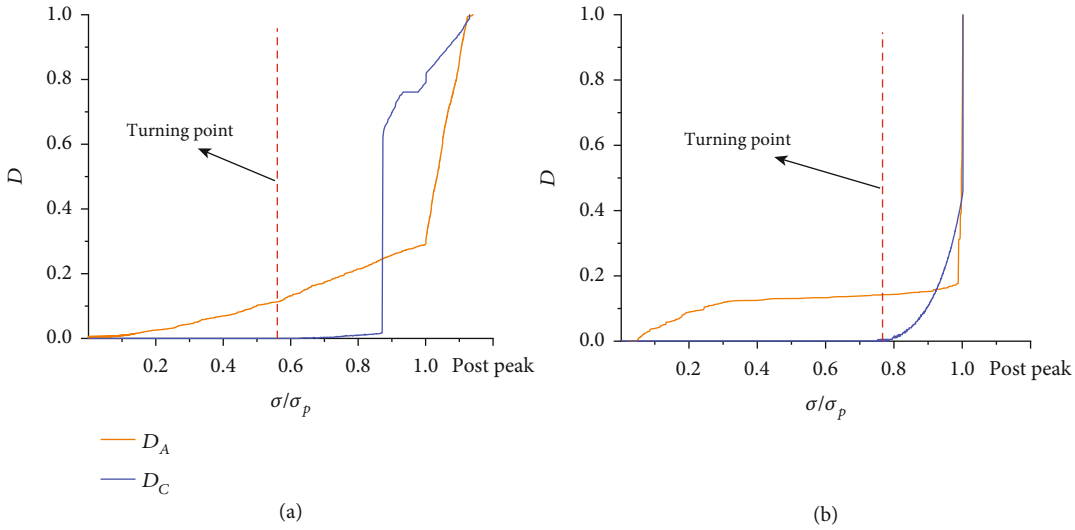

Figure 11: Damage variable curve of the sandstone samples from different depths under uniaxial compression: (a) 350 m; (b) 750 m.

as the starting point of the fracture volume's expansion and the damage before the Turning Point is ignored. The damage variable D_c characterized by the volume strain of the fracture can be defined as

$$D_c = \begin{cases} 0 & t < t_t \\ \dfrac{\varepsilon_c - \varepsilon_{ct}}{\varepsilon_{cm} - \varepsilon_{ct}} & t > t_t \end{cases}, \tag{10}$$

where ε_c is the crack volumetric strain during the damage process, ε_{ct} is the crack volumetric strain corresponding to the Turning Point (i.e., the maximum compressive crack volumetric strain), ε_{cm} is the crack volumetric strain at the end of the experiment (i.e., the maximum expansion crack volumetric strain), and t_t is the loading time point corresponding to the Turning Point. The evolution law of the damage variables calculated by Equations (9) and (10) in the loading process is shown in Figure 11.

The damage variable D_c is closely related to the generation and types of cracks and is analyzed in detail in the subsequent sections. The essence of the damage variable D_A is the change law of the cumulative AE ring count, and the AE signal originates from the interior of the rock. It is a transient event caused by a local unstable state, which reflects the characteristics of the rock itself. The evolution law of the damage variable D_A of the rock samples at different depths is obviously different. The damage variable of the sandstone samples from the 750 m depth is less than 20% before failure, while the sandstone samples from the 350 m depth show a sustained and stable damage increase in the entire loading stage. This indicates that plastic slip dislocation occurs between the sandstone grains in the samples from the 350 m depth before peak stress and that the internal structure has been cracked. The structure of the sandstones from 750 m deep did not change significantly after compression except for a fracture appearing near the macroscopic fracture surface. This also shows to some extent that the sandstones from the 750 m depth have a uniform texture with no obvious anisotropy. Whether there is plastic deformation before the peak and, if so, what the scope and degree of the plastic deformation are two of the main criteria to determine whether brittle failure of the rock will occur. The occurrence of plastic deformation before the peak stress may be related to the difference in the rock's mineral composition at different depths [66, 67]. Different mineral compositions have different particle sizes, strength parameters (strength, elastic modulus, Poisson's ratio, thermal expansion coefficient, etc.), and properties (brittleness degree) [68]. The strength and brittleness of mineral components determine the proportion of transcrystalline and intergranular cracks and the specific surface energy and shear crack energy required for tensile and shear crack. Figure 12 shows the X-ray diffraction results of rock samples from the two different depths.

The brittle mineral content of the sandstones from the two depths is very high, but the quartz content in the sandstones from the 750 m depth is significantly higher than that in the sandstones from the 350 m depth, and the sandstone from the 750 m depth does not contain kaolinite. The high quartz content in the sandstone from the 750 m depth makes it stronger than the sandstone from the 350 m depth, and the brittleness of quartz particles is high, which makes the rock prone to brittle fracture. The shallow buried sandstone contains kaolinite, and the muscovite content of low strength relative to quartz is higher, which makes it easier for these areas to become the location for the initiation of microcracks.

Based on the above analysis, the damage variable D_A can be used to better distinguish the physical properties of the rock at the two different depths and can help to better judge the brittleness and anisotropy of the rock. Even if the failure processes of the specimens from different depths are quite different, the two kinds of damage variables have

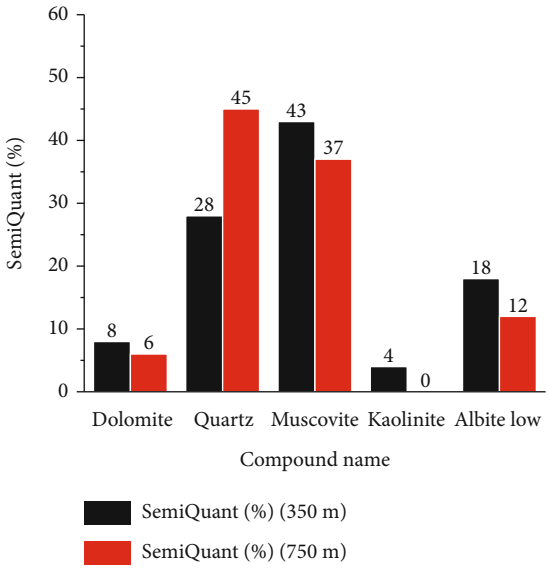

FIGURE 12: Composition analysis table of samples from the 350 m depth and 750 m depth.

different emphases. Combined with the analysis of the two curves of the damage variables, the damage evolution of the sandstone during uniaxial compression can be well characterized.

5. Discussion

5.1. Influence of Buried Depth on the Failure Properties of Sandstone. As mentioned above, there are some differences in the essential physical properties of the sandstones at different depths in the same borehole of the tunnel, and then, there are significant differences in the brittle characteristics, acoustic emission characteristics, mechanical properties, damage evolution, and other aspects obtained during the uniaxial compression process. At the macroscale, the differences in the essential physical properties are mainly reflected in the differences in the failure process of the sandstones from different depths. Rock mechanics in the process of rock failure can be regarded as the mechanical behavior of the fractured rock mass on the engineering scale. In particular, the strength distribution, deformation characteristics, and failure evolution of a fractured rock mass under load are related to the initiation, development, expansion, and penetration of internal microcracks at the microscopic scale. The development of microcracks during rock damage affects the propagation of surface macrocracks [69, 70]. Therefore, the influence of buried depth on the failure properties of sandstone depends to a large extent on the types of microcracks generated in the rock and the development process of the microcracks. The crack type in a rock can be determined by AE parameters and the RA and AF values [71]. Combining RA and AF values with the macroscopic and microscopic failure characteristics of sandstone can help to better explain the initiation, propagation, and penetration of different types of cracks in the sandstone at different depths; this is important when performing a damage analysis of the sandstone. The calculation formulas of RA and AF are as follows [72]:

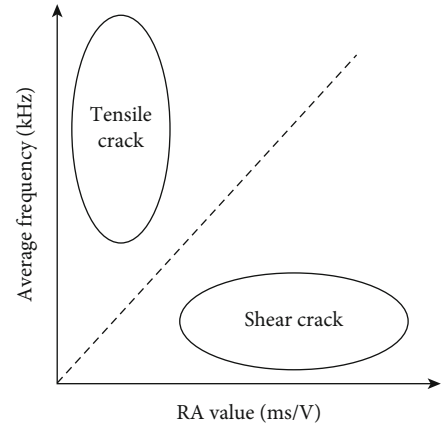

FIGURE 13: Relationship between average frequency and RA value [72].

$$\text{RA value} = \frac{\text{the rise time}}{\text{the maximum amplitude}},$$
$$\text{The average frequency (AF)} = \frac{\text{AE ringdown} - \text{count}}{\text{the duration time}}. \quad (11)$$

Tensile cracks have high RA values and low AF values; on the contrary, shear cracks have low RA values and high AF values. This crack classification method is based on the JCMS-III B5706 code, of which results were confirmed under the four-point bending tests and the direct shear tests of concrete specimens (Figure 13).

Based on the study of Ohtsu [72], Liu et al. [73], and Lotidis and Nomikos [74], the microcracks in sandstones at different depths during uniaxial compression were classified by RA-AF correlation analysis (AF: RA = 2). The results were combined with the fractal dimension, as shown in Figure 14.

In the peak stress stage ($80\%\sigma_p \sim 100\%\sigma_p$) and the post-peak stress stage ($100\%\sigma_p \sim 80\%\sigma_p$), the proportion of shear cracks in the sandstone samples is higher than that in the previous stress stages. At the same time, it is observed that the cracks in the sandstone samples from the 350 m depth gradually change from tensile cracks to shear cracks in the loading process, and the proportion of shear cracks is more than 50% when the fractal dimension reaches the minimum. However, when the fractal dimension of the sandstone sample from the 750 m depth reaches the minimum, the proportion of shear cracks is 0%, and the tensile cracks always dominate the loading process. But when the fractal dimension of the sandstone samples from the 750 m depth reaches the minimum, the proportion of shear cracks is 0%, and the tensile cracks always dominate the loading process. When the fractal dimension is the smallest (Turning Point position), the cracks in the rock have been compacted, and the continuous loading leads to the accumulation of dislocations

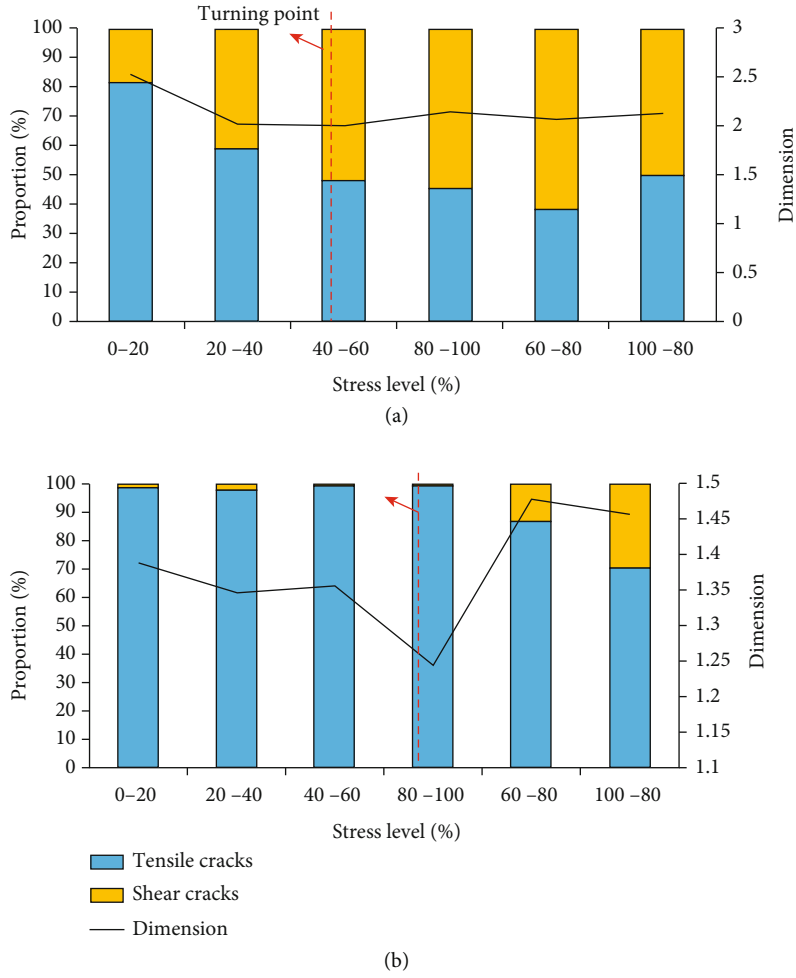

Figure 14: Dimension evolution and proportion of tensile cracks and shear cracks under different stress levels: (a) 350 m; (b) 750 m.

in the sandstone crystals on the grain boundaries. With the continuous accumulation of defects, the main fracture surface initiates. The subsequent loading causes the penetration and extension of the main fracture surface formed at this time until failure. Therefore, what kind of crack dominates when the Turning Point is reached will determine the ultimate failure properties of the rock. At this time, the proportion of shear cracks generated in the sandstones from the 350 m depth is more than half. These shear cracks make all kinds of microcracks connect with each other. At the same time, new shear cracks are generated, forming a shear plane that is not parallel to the axial direction. If there is only a small number of shear cracks or even no shear cracks, then under the action of load, the tensile microcracks continue to propagate parallel to the axial direction, and a penetrating crack surface parallel to the axial direction will form in the subsequent failure process. It can be seen that the proportion of shear cracks plays a decisive role in the expansion of internal cracks and the failure process of sandstone in this tunnel. At the same time, it is also consistent with the speculation of 3.2.

The shear crack ratio in the sandstone samples from the 350 m depth continues to increase after the Turning Point and decreases in the postpeak stage. The curve slope of the damage variable D_c shows an increasing trend in the failure process until it suddenly decreases to failure in the postpeak stage. The shear crack ratio of the sandstone samples from the 750 m depth increases continuously after the fractal dimension reaches the minimum value, which is reflected in the curve of damage variable D_c where the slope begins to grow rapidly after a gentle period. The shear crack ratio of the sandstone samples from the 750 m depth increases sharply in the postpeak stage, and the growth rate of the corresponding damage variable D_c also increases to a certain high level until the end of the experiment. When the proportion of shear cracks reaches the maximum in the sandstones from the different buried depths, the curve of the damage variable D_c is close to vertical. At this time, plenty of cracks penetrate the samples, a large fracture surface expands, and the instability of the rock follows. It can be seen that the damage variable D_c characterized by the crack volumetric strain has a good correlation with the proportion of shear cracks. The higher the proportion of shear cracks generated in the sandstone samples from the same depth in a certain loading stage, the higher the degree of crack penetration, and the higher the rate of damage growth.

The rocks at different depths selected in this paper are all intact rocks with good homogeneity, and the influence of the structural plane can be approximately ignored. Considering the microscopic crack initiation and macroscopic failure performance, the samples from the 750 m depth have higher strength, elastic modulus, compactness, brittleness, and a higher proportion of tensile cracks in the failure process than the samples from the 350 m depth. The failure type of the former is mainly tensile failure without the general positive acoustic emission phenomenon of the latter. Combining the damage evolution curves and the fractal dimension curves shows that damage of the sandstones from the 750 m depth is more sudden with more obvious signal representation when reaching the Turning Point and peak stress.

5.2. Engineering Effects of the Turning Point in the Process of Rock Failure. The study on the characteristic parameters of the entire process of failure of the surrounding rock from a railway tunnel in the Qinghai-Tibet Plateau under uniaxial compression reveals the relationship between rock failure, acoustic emission, and the physical parameters of the rock from different depths. In high-altitude areas, the surrounding rocks with deep buried depths are in high initial in situ stress, and the rock mass around the cavern is a generally high-strength brittle hard rock. The rock mass will show brittle failure, causing the rock mass to frequently experience violent damage such as ejection, expansion, collapse, and even rock burst when unloading occurs by the mining disturbance. For the engineering disasters in high-altitude and high in situ stress areas, further research is still underway. The study on the mechanical behavior of rocks at different depths is helpful to further understand the failure mechanism of surrounding rocks in tunnels and propose reasonable precursor criteria to predict or judge rock failure; this is of great significance when implementing tunnel engineering with a large depth span.

In the process of rock compression or disturbance, the compression and penetration of cracks were carried out synchronously. The Turning Point in this paper is the point at which the crack volumetric strain state changed from compression to expansion. In previous studies, the stress corresponding to the Turning Point is called the crack initiation stress, and it is believed that the rock begins to crack at this time. However, it can be seen from the research in this paper that different kinds of microcracks have been continuously generated and compressed through acoustic emission monitoring and fractal dimension calculation and analysis, before the rock reached the Turning Point. When reaching the Turning Point, microscopically, the generation or penetration rate of cracks exceeds the rate of compression, but macroscopically, it is manifested as rock cracking. At the same time, the fractal dimension reached the lowest level, and the behavior of cracks became orderly and began to concentrate on the weak surface or the crack surface. Hence, at the Turning Point, which microcrack type (tensile/shear) is dominant will determine the failure mode of the rock, and these cracks will initiate penetrating cracks according to the potential main fracture plane. Since then, the internal structure of the rock has undergone irreversible changes due to the rapid expansion and penetration of cracks. Many scholars also defined the crack initiation stress point as the starting point of the plastic stage. From the analysis of this paper, this is quite correct. Moreover, the Turning Point can be used to divide the two to facilitate subsequent analysis when the plastic stage and the elastic stage are not clearly distinguished in the rock stress-strain curves, such as plastic deformation analysis, energy calculation, and brittleness index calculation.

The Turning Point can help to predict some key failure areas or burst points in engineering rock masses. In tunnel excavation engineering under high in situ stress conditions, without support, the rock near the tunnel wall exists in a uniaxial compression state due to stress concentration, and σ_{ci} is a parameter independent of size and can reflect the characteristics of rock materials at depth.

6. Conclusion

(1) After reaching peak stress, sandstones from the 350 m depth show a ladder type of instability failure. The sandstones from the 750 m depth are destroyed rapidly after reaching peak stress and show great brittleness. At the same time, the elastic modulus and uniaxial compressive strength of sandstones from the 750 m depth are significantly higher than those of the sandstones from the 350 m depth. The number of acoustic emission events in the sandstones from the 350 m depth is significantly larger than that in the sandstones from the 750 m depth, but the proportion of acoustic emission events in the 10^2~104 aJ (10^{-18} J) energy level is significantly lower than that in the sandstones from the 750 m depth

(2) The fractal dimension of the sandstones from the 750 m depth maintained a low level (less than 1.5) during the entire loading process, which is significantly lower than that of the sandstones from the 350 m depth. This shows that the overall evolution of internal cracks in deep rock samples is more orderly and stable and that their distribution is more concentrated. As a result, the sandstone from the 750 m depth shows sudden instability failure characteristics

(3) During the loading process, the crack type in the sandstones from the 350 m depth gradually transform from tensile cracks to shear cracks, and the proportion of shear cracks generated when the fractal dimension reaches the minimum is greater than 50%. However, when the fractal dimension of the sandstones from the 750 m depth reaches the minimum value, the proportion of shear cracks is 0%, and the tensile cracks always dominate in the loading process. As a result, the final failure mode and failure characteristics of the sandstones from the different depths are different. The time point when the crack volumetric strain changes from compression to expansion coincides with the lowest point of the

fractal dimension, which indicates that the main fracture surface or the main cracks have been initiated at this time and determine the future shear or tensile failure of the rock. Thus, the failure characteristics of the sandstones can be predicted by monitoring the acoustic emission characteristics at the Turning Point

(4) The damage variable D_c based on the crack volumetric strain theory can better reflect the generation and penetration of cracks in a rock and can better reflect the effect and influence of different types of cracks on rock damage. The damage variable D_A based on the cumulative ring count of acoustic emission can help to better distinguish the physical properties of rocks at two different depths and can help to better judge the brittleness and anisotropy of a rock mass. Therefore, the damage evolution of sandstones in the tunnels in Qinghai-Tibet Plateau can be analyzed by combining these two damage variables

Data Availability

The data that support the findings of this study are available from the corresponding authors upon reasonable request.

Conflicts of Interest

No conflict of interest exists in the submission of this manuscript.

Acknowledgments

This study was supported by the National Natural Science Foundation of China (Grant No. 52125402) and the open fund of Key Laboratory of Deep Earth Science and Engineering (Sichuan University), Ministry of Education (Grant No. DESE202104).

References

[1] L. G. Xu, F. M. Kong, W. M. Yang et al., "Main unfavorable geological conditions and engineering geological problems along Sichuan—Tibet railway," *Chinese Journal of Rock Mechanics and Engine*, vol. 39, no. 3, pp. 445–468, 2019.

[2] G. Feng, Y. Kang, X. C. Wang, Y. Q. Hu, and X. H. Li, "Investigation on the failure characteristics and fracture classification of shale under brazilian test conditions," *Rock Mechanics and Rock Engineering*, vol. 53, no. 7, pp. 3325–3340, 2020.

[3] B. L. A. Isaka, P. G. Ranjith, T. D. Rathnaweera, M. S. A. Perera, and W. G. P. Kumari, "Influence of long-term operation of supercritical carbon dioxide based enhanced geothermal system on mineralogical and microstructurally-induced mechanical alteration of surrounding rock mass," *Renewable Energy*, vol. 136, pp. 428–441, 2019.

[4] T. Meng, J. L. Xie, X. M. Li, J. W. Ma, and Y. Yue, "Experimental study on the evolutional trend of pore structures and fractal dimension of low-rank coal rich clay subjected to a coupled thermo-hydro-mechanical-chemical environment," *Energy*, vol. 203, article 117838, 2020.

[5] S. Mei and D. L. Kohlstedt, "Influence of water on plastic deformation of olivine aggregates 2. Dislocation creep regime," *Journal of Geophysical Research: Solid Earth*, vol. 105, no. B9, pp. 21471–21481, 2000.

[6] J. Chen, X. L. Shi, and J. K. Zhou, "The mechanical characteristic of rock salt under uniaxial compression with low temperature effect," *Functional Materials*, vol. 23, no. 3, pp. 433–436, 2016.

[7] C. Zhai, X. W. Xiang, J. Z. Xu, and S. L. Wu, "The characteristics and main influencing factors affecting coal and gas outbursts in Chinese Pingdingshan mining region," *Natural Hazards*, vol. 82, no. 1, pp. 507–530, 2016.

[8] Z. A. Erguler and R. Ulusay, "Water-induced variations in mechanical properties of clay-bearing rocks," *International Journal of Rock Mechanics and Mining Sciences*, vol. 46, no. 2, pp. 355–370, 2009.

[9] Q. Yin, J. Y. Wu, Z. Jiang et al., "Investigating the effect of water quenching cycles on mechanical behaviors for granites after conventional triaxial compression," *Geomechanics and Geophysics for Geo-Energy and Geo-Resources*, vol. 8, no. 2, p. 77, 2022.

[10] D. H. Chen, H. E. Chen, W. Zhang, J. Q. Lou, and B. Shan, "An analytical solution of equivalent elastic modulus considering confining stress and its variables sensitivity analysis for fractured rock masses," *Journal of Rock Mechanics and Geotechnical Engineering*, vol. 14, no. 3, pp. 825–836, 2022.

[11] G. Feng, Y. Kang, T. Meng, Y.-q. Hu, and X.-h. Li, "The influence of temperature on mode I fracture toughness and fracture characteristics of sandstone," *Rock Mechanics and Rock Engineering*, vol. 50, no. 8, pp. 2007–2019, 2017.

[12] G. Feng, Y. Kang, F. Chen, Y.-w. Liu, and X.-c. Wang, "The influence of temperatures on mixed-mode (I + II) and mode-II fracture toughness of sandstone," *Engineering Fracture Mechanics*, vol. 189, pp. 51–63, 2018.

[13] Y. Wang, W. K. Feng, R. L. Hu, and C. H. Li, "Fracture evolution and energy characteristics during marble failure under triaxial fatigue cyclic and confining pressure unloading (FC-CPU) conditions," *Rock Mechanics and Rock Engineering*, vol. 54, no. 2, pp. 799–818, 2021.

[14] P. Jin, Y. Hu, J. Shao, Z. Liu, G. Feng, and S. Song, "Influence of temperature on the structure of pore–fracture of sandstone," *Rock Mechanics and Rock Engineering*, vol. 53, no. 1, pp. 1–12, 2019.

[15] J. Xu, Y. Kang, X. Wang, G. Feng, and Z. Wang, "Dynamic characteristics and safety criterion of deep rock mine opening under blast loading," *International Journal of Rock Mechanics and Mining Sciences*, vol. 119, pp. 156–167, 2019.

[16] H. P. Xie, M. Z. Gao, R. Zhang, G. Y. Peng, W. Y. Wang, and A. Q. Li, "Study on the mechanical properties and mechanical response of coal mining at 1000 m or deeper," *Rock Mechanics and Rock Engineering*, vol. 52, pp. 1475–1490, 2018.

[17] Z. T. Zhang, R. Zhang, S. Y. Wu, J. H. Deng, Z. P. Zhang, and J. Xie, "The stress sensitivity and porosity sensitivity of coal permeability at different depths: a case study in the Pingdingshan mining area," *Rock Mechanics and Rock Engineering*, vol. 52, no. 5, pp. 1539–1563, 2019.

[18] Z. Q. Jia, C. B. Li, R. Zhang et al., "Energy evolution of coal at different depths under unloading conditions," *Rock Mechanics and Rock Engineering*, vol. 52, no. 11, pp. 4637–4649, 2019.

[19] Y. Q. Lu, C. Li, Z. Q. He et al., "Variations in the physical and mechanical properties of rocks from different depths in the

Songliao Basin under uniaxial compression conditions," *Geomechanics and Geophysics for Geo-Energy and Geo-Resources*, vol. 6, no. 43, 2020.

[20] C. D. Martin, "Seventeenth Canadian geotechnical colloquium: the effect of cohesion loss and stress path on brittle rock strength," *Canadian Geotechnical Journal*, vol. 34, no. 5, pp. 698–725, 1997.

[21] W. Gao, S. Dai, T. Xiao, and T. Y. He, "Failure process of rock slopes with cracks based on the fracture mechanics method," *Engineering Geology*, vol. 231, pp. 190–199, 2017.

[22] G. Feng, X. Wang, Y. Kang, and Z. Zhang, "Effect of thermal cycling-dependent cracks on physical and mechanical properties of granite for enhanced geothermal system," *International Journal of Rock Mechanics and Mining Sciences*, vol. 134, article 104476, 2020.

[23] G. Feng, X. Wang, M. Wang, and Y. Kang, "Experimental investigation of thermal cycling effect on fracture characteristics of granite in a geothermal-energy reservoir," *Engineering Fracture Mechanics*, vol. 235, article 107180, 2020.

[24] A. J. Tang, C. G. Shi, Y. Wang, and J. H. Wang, "Energy characteristics of brittle rock in failure process," *Applied Mechanics and Materials*, vol. 580-583, pp. 260–273, 2014.

[25] V. Hajiabdolmajid, P. K. Kaiser, and C. D. Martin, "Modelling brittle failure of rock," *International Journal of Rock Mechanics and Mining Sciences*, vol. 39, no. 6, pp. 731–741, 2002.

[26] Z.'a. Wang, Y. Kang, F. Xie et al., "Experimental investigation on the penetration characteristics of low-frequency impact of pulsed water jet," *Wear*, vol. 488-489, article 204145, 2022.

[27] C. Zhu, M. Karakus, M. C. He et al., "Volumetric deformation and damage evolution of Tibet interbedded skarn under multistage constant-amplitude-cyclic loading," *International Journal of Rock Mechanics and Mining Sciences*, vol. 152, article 105066, 2022.

[28] Y. Q. Su, F. Q. Gong, S. Luo, and Z. X. Liu, "Experimental study on energy storage and dissipation characteristics of granite under two-dimensional compression with constant confining pressure," *Journal of Central South University*, vol. 28, no. 3, pp. 848–865, 2021.

[29] Y. Wang, S. H. Gao, Q. D. Liu, and C. H. Li, "Anisotropic fatigue behaviour of interbeded marble subjected to uniaxial cyclic compressive loads," *Fatigue & Fracture of Engineering Materials & Structures*, vol. 43, no. 6, pp. 1170–1183, 2020.

[30] Z. J. Wu, Z. Y. Wang, L. F. Fan, L. Weng, and Q. S. Liu, "Micro-failure process and failure mechanism of brittle rock under uniaxial compression using continuous real-time wave velocity measurement," *Journal of Central South University*, vol. 28, no. 2, pp. 556–571, 2021.

[31] Y. Wang, D. Q. Liu, J. Q. Han, C. H. Li, and H. Liu, "Effect of fatigue loading-confining stress unloading rate on marble mechanical behaviors: an insight into fracture evolution analyses," *Journal of Rock Mechanics and Geotechnical Engineering*, vol. 12, no. 6, pp. 1249–1262, 2020.

[32] Y. Wang, W. K. Feng, and C. H. Li, "On anisotropic fracture and energy evolution of marble subjected to triaxial fatigue cyclic-confining pressure unloading conditions," *International Journal of Fatigue*, vol. 134, article 105524, 2020.

[33] M. Gao, H. Haichun, S. Xue et al., "Discing behavior and mechanism of cores extracted from Songke-2 well at depths below 4,500m," *International Journal of Rock Mechanics and Mining Sciences*, vol. 149, article 104976, 2022.

[34] M.-Z. Gao, B.-G. Yang, J. Xie et al., "The mechanism of microwave rock breaking and its potential application to rock-breaking technology in drilling," *Petroleum Science*, vol. 19, no. 3, pp. 1110–1124, 2022.

[35] M.-Z. Gao, J.-G. Zhang, S.-W. Li, M. Wang, Y.-w. Wang, and P.-F. Cui, "Calculating changes in fractal dimension of surface cracks to quantify how the dynamic loading rate affects rock failure in deep mining," *Journal of Central South University of Technology*, vol. 27, no. 10, pp. 3013–3024, 2020.

[36] M. Mabuza, K. Premlall, and M. O. Daramola, "Modelling and thermodynamic properties of pure CO_2 and flue gas sorption data on South African coals using Langmuir, Freundlich, Temkin, and extended Langmuir isotherm models," *International Journal of Coal Science & Technology*, vol. 9, no. 1, p. 45, 2022.

[37] T. Meng, L. Ma, F. Wu, F. Gan, and Y. Xue, "Experimental study on permeability evolution and nonlinear seepage characteristics of fractured rock in coupled thermo-hydraulic-mechanical environment:a case study of the sedimentary rock in Xishan area," *Engineering Geology*, vol. 294, article 106339, 2021.

[38] P. Jin, Y. Hu, J. Shao, G. Zhao, X. Zhu, and C. Li, "Influence of different thermal cycling treatments on the physical, mechanical and transport properties of granite," *Geothermics*, vol. 78, pp. 118–128, 2019.

[39] F. Q. Ren, C. Zhu, and M. C. He, "Moment tensor analysis of acoustic emissions for cracking mechanisms during schist strain burst," *Rock Mechanics and Rock Engineering*, vol. 53, no. 1, pp. 153–170, 2020.

[40] G. C. Shi, X. J. Yang, H. C. Yu, and C. Zhu, "Acoustic emission characteristics of creep fracture evolution in double-fracture fine sandstone under uniaxial compression," *Engineering Fracture Mechanics*, vol. 210, pp. 13–28, 2019.

[41] L. Dou, K. Yang, and X. Chi, "Fracture behavior and acoustic emission characteristics of sandstone samples with inclined precracks," *International Journal of Coal Science and Technology*, vol. 8, no. 1, pp. 77–87, 2021.

[42] B. Liu, Y. Zhao, C. Zhang, J. Zhou, Y. Li, and Z. Sun, "Characteristic strength and acoustic emission properties of weakly cemented sandstone at different depths under uniaxial compression," *International Journal of Coal Science and Technology*, vol. 8, no. 6, pp. 1288–1301, 2021.

[43] Y. Deng, Y. Liu, and D.-m. Feng, "Monitoring damage evolution of steel strand using acoustic emission technique and rate process theory," *Journal of Central South University*, vol. 21, no. 9, pp. 3692–3697, 2014.

[44] Q.-b. Lin, P. Cao, K.-h. Li, R.-h. Cao, K.-p. Zhou, and H.-w. Deng, "Experimental study on acoustic emission characteristics of jointed rock mass by double disc cutter," *Journal of Central South University*, vol. 25, no. 2, pp. 357–367, 2018.

[45] D. A. Lockner, J. D. Byerlee, V. Kuksenko, A. Ponomarev, and A. Sidorin, "Quasi-static fault growth and shear fracture energy in granite," *Nature*, vol. 350, no. 6313, pp. 39–42, 1991.

[46] D. A. Lockner, "The role of acoustic emission in the study of rock fracture," *International Journal of Rock Mechanics and Mining Sciences & Geomechanics Abstracts*, vol. 30, no. 7, pp. 883–899, 1993.

[47] M. C. He, J. L. Miao, and J. L. Feng, "Rock burst process of limestone and its acoustic emission characteristics under true-triaxial unloading conditions," *International Journal of Rock Mechanics and Mining Sciences*, vol. 47, no. 2, pp. 286–298, 2010.

[48] Y. X. Zhao, X. L. Wang, Y. D. Guo, and X. J. Hao, "Brittleness index of sandstones from different buried depths based on energy release rate," *Chinese Journal of Rock Mechanics and Engine*, vol. 40, no. 2, pp. 248–262, 2021.

[49] A. H. Cottrell, "Theory of brittle fracture in steel and similar metals," *Transactions of The American Institute of Mining And Metallurgical Engineers*, vol. 212, pp. 192–203, 1958.

[50] Y. Wang, C. H. Li, Y. Z. Hu, and X. L. Zhou, "A new method to evaluate the brittleness for brittle rock using crack initiation stress level from uniaxial stress–strain curves," *Environmental Earth Sciences*, vol. 76, no. 23, p. 799, 2017.

[51] Y. Wang, W. H. Tan, D. Q. Liu, Z. Q. Hou, and C. H. Li, "On anisotropic fracture evolution and energy mechanism during marble failure under uniaxial deformation," *Rock Mechanics and Rock Engineering*, vol. 52, no. 10, pp. 3567–3583, 2019.

[52] C. D. Martin and N. A. Chandler, "The progressive fracture of Lac du Bonnet granite," *International Journal of Rock Mechanics and Mining Sciences*, vol. 31, no. 6, pp. 643–659, 1994.

[53] M. Cai, P. K. Kaiser, Y. Tasaka, T. Maejima, H. Morioka, and M. Minami, "Generalized crack initiation and crack damage stress thresholds of brittle rock masses near underground excavations," *International Journal of Rock Mechanics and Mining Sciences*, vol. 41, no. 5, pp. 833–847, 2004.

[54] R. A. Everitt and E. Z. Lajtai, "The influence of rock fabric on excavation damage in the Lac du Bonnett granite," *International Journal of Rock Mechanics and Mining Sciences*, vol. 41, no. 8, pp. 1277–1303, 2004.

[55] H. P. Xie, *Introduction to Fractals - Rock Mechanics*, Science Press, Beijing, 1996.

[56] M. L. Chen, H. W. Jing, X. J. Ma, H. J. Su, M. R. Du, and T. T. Zhu, "Fracture evolution characteristics of sandstone containing double fissures and a single circular hole under uniaxial compression," *International Journal of Mining Science and Technology*, vol. 27, no. 3, pp. 499–505, 2017.

[57] N. H. Wu, H. P. Xie, L. Chen, M. Z. Gao, and C. Li, "Sealing form and failure mechanism of deep in situ rock core pressure-maintaining controller," *Geofluids*, vol. 2020, Article ID 8892720, 15 pages, 2020.

[58] H. P. Xie, T. Liu, M. Z. Gao et al., "Research on in-situ condition preserved coring and testing systems," *Petroleum Science*, vol. 18, no. 6, pp. 1840–1859, 2021.

[59] H. P. Xie, C. Li, Z. Q. He et al., "Experimental study on rock mechanical behavior retaining the in situ geological conditions at different depths," *International Journal of Rock Mechanics and Mining Sciences*, vol. 138, article 104548, 2021.

[60] X. D. Xu, M. C. He, C. Zhu, Y. Lin, and C. Cao, "A new calculation model of blasting damage degree–Based on fractal and tie rod damage theory," *Engineering Fracture Mechanics*, vol. 220, article 106619, 2019.

[61] Z. Yang, H. Zhou, J. Zhong, and D. Liu, "Study on the relation between damage and permeability of sandstone at depth under cyclic loading," *International Journal of Coal Science and Technology*, vol. 6, no. 4, pp. 479–492, 2019.

[62] X. U. Xiao-li, K. A. R. A. K. U. S. Murat, G. A. O. Feng, and Z. H. A. N. G. Zhi-zhen, "Thermal damage constitutive model for rock considering damage threshold and residual strength," *Journal of Central South University*, vol. 25, pp. 2523–2536, 2018.

[63] L. M. Kachanov, "Introduction to Continuum Damage Mechanics," in *Mechanics of Elastic Stability*, Brookline, Dordrecht, 1986.

[64] Y. J. Zong, L. J. Han, J. J. Wei, and S. Y. Wen, "Mechanical and damage evolution properties of sandstone under triaxial compression," *International Journal of Rock Mechanics and Mining Sciences*, vol. 26, no. 4, pp. 601–607, 2016.

[65] Y. J. Zong, L. J. Han, Q. B. Meng, and Y. C. Wang, "Strength properties and evolution laws of cracked sandstone samples in re-loading tests," *International Journal of Mining Science and Technology*, vol. 30, no. 2, pp. 251–258, 2020.

[66] H. M. Li, H. G. Li, K. L. Wang, and C. Liu, "Effect of rock composition microstructure and pore characteristics on its rock mechanics properties," *International Journal of Mining Science and Technology*, vol. 28, no. 2, pp. 303–308, 2018.

[67] Y. L. Chen, Q. B. Meng, G. Xu, H. S. Wu, and G. M. Zhang, "Bolt-grouting combined support technology in deep soft rock roadway," *International Journal of Mining Science and Technology*, vol. 26, no. 5, pp. 777–785, 2016.

[68] G. C. Li, Z. H. Jiang, C. X. Lv, C. Huang, G. Chen, and M. Y. Li, "Instability mechanism and control technology of soft rock roadway affected by mining and high confined water," *International Journal of Mining Science and Technology*, vol. 25, no. 4, pp. 573–580, 2015.

[69] J. Yang, S. Q. Yang, G. J. Liu, W. L. Tian, and Y. Li, "Experimental study of crack evolution in prefabricated double-fissure red sandstone based on acoustic emission location," *Geomech Geophys Geo-Energy Geo-Resour*, vol. 7, no. 1, 2021.

[70] Z. Agioutantis, K. Kaklis, S. Mavrigiannakis, M. Verigakis, F. Vallianatos, and V. Saltas, "Potential of acoustic emissions from three point bending tests as rock failure precursors," *International Journal of Mining Science and Technology*, vol. 26, no. 1, pp. 155–160, 2016.

[71] K. Ohno and M. Ohtsu, "Crack classification in concrete based on acoustic emission," *Construction and Building Materials*, vol. 24, no. 12, pp. 2339–2346, 2010.

[72] M. Ohtsu, T. Okamoto, and S. Yuyama, "Moment tensor analysis of acoustic emission for cracking mechanisms in concrete," *ACI Structural Journal*, vol. 95, no. 2, pp. 87–95, 1998.

[73] Y. B. Liu, G. Z. Yin, M. H. Li et al., "Mechanical properties and failure behavior of dry and water-saturated anisotropic coal under true-triaxial loading conditions," *Rock Mechanics and Rock Engineering*, vol. 53, no. 11, pp. 4799–4818, 2020.

[74] M. A. Lotidis and P. P. Nomikos, "Acoustic emission location analysis and microcracks' nature determination of uniaxially compressed calcitic marble hollow plates," *Geomechanics and Geophysics for Geo-Energy and Geo-Resources*, vol. 7, no. 2, 2021.